This version published 07/01/2025 replaces the previous version published 10/01/2024 to improve the formatting of the equations.

Supporting Information: The solubility product controls the rate of calcite dissolution in pure water and seawater

Authors: Minjun Yang,[1†] Ling Tan,[1†] Christopher Batchelor-McAuley[2], Richard G. Compton[1*]

Affiliations:

[1] Physical and Theoretical Chemistry Laboratory, Department of Chemistry, University of Oxford; South Parks Road, Oxford, Great Britain

[2] The School of Chemistry, Trinity College Dublin, The University of Dublin. College Green, Dublin 2, Ireland

*Corresponding author. E-mail: Richard.Compton@chem.ox.ac.uk

†These authors contributed equally to this work

SI Section 1. Mucci's approach to measuring the stoichiometric solubility product

The stoichiometric solubility product of calcite was established from long term equilibration of solid calcite particles with seawater as reported by Mucci[1, 2]. In particular it is insightful to note three features of these experiments. First that in Mucci's long term equilibrium experiments, prior to the experiment, the salinity of the seawater was altered from its original salinity (36.5%) to the desired salinity by either the addition of deionised water or by evaporation; simultaneously the levels of dissolved calcium ions were diluted. Second, the resultant seawater was made undersaturated with respect to calcite by the addition of acid prior to the 'long term equilibrium' experiment. The addition of acid protonates and hence reduces the concentration of carbonate, $[CO_3^{2-}]$, forming HCO_3^- to result in a proportionate decrease in the calcite saturation state (Ω). By adding an excess amount of analytical grade calcite particles and waiting (patiently!) for a long time, ranging from 5 days to almost 2 years, a 'long term equilibrium' was eventually deemed established and the solution composition measured as a function of seawater salinity were reported.[2] Note that the final solutions contain calcium levels reflecting not only the initial calcium ions present in the diluted seawater but also additionally those dissolved during the period of equilibration. Third, and importantly, Mucci, and indeed most of the oceanography community for similar measurements[1, 3-5], used titration to analyse the concentrations of Ca^{2+} and of CO_3^{2-} in the equilibrated solutions. This includes EGTA titration of $[Ca^{2+}]$ and, separately, calculating $[CO_3^{2-}]$ from pH and alkalinity measurements, where the latter involves measuring the amount of acid required to bring the seawater medium to pH 4.5. Thus, in the absence of any corrections, the measured concentrations are the *total concentrations* of the constituent ions including the free ions and those ions paired.[2] Mucci reports the apparent stoichiometric solubility constant, $K^0_{sp,apparent}$ in terms of the *total* concentrations of calcium and carbonate (Eqn 2 in the main manuscript). To infer the true

stoichiometric solubility constant, $K_{sp}{}^{0}$, however, it is necessary to account and correct for ion pairings.

SI Section 2. Materials and Methods

Materials

Deionised water used was Mili-Q ultrapure water with resistivity of 18.2 MΩ cm at 25 °C. $NaHCO_3$ and Na_2CO_3 were bought from Acros Organics; $CaCl_2$ from Aldrich. The calcite particles used in the experiments were synthesised[6] via precipitation from a mixture of supersaturated calcium chloride and disodium carbonate solutions. X-ray diffraction and scanning electron microscopy characterisation, reported elsewhere,[6] concluded the formation of pristine micron-sized calcite particles.

Optical Microscopy measurements

A 20x objective (Olympus UPLXAPO 20x, Olympus Corporation, Tokyo Japan) was used for the optical measurements. The illumination was applied by a LED Illuminator (Aura Pro Phase Contrast Illuminator, Cairn Research, Kent U.K.) and ORCA-Flash 4.0 digital camera (C13440-20CU, Hamamatsu Photonics, Japan) acquired the images. The black-and-white images were of size 16 bits with an exposure time of 400 ms.

The images were analyzed by the ImageJ freeware (Fiji). The projected area of each calcite particle in pixels is determined by using the auto-thresholding functions within the ImageJ freeware. The actual projected area is the number of pixels in the 2-D image multiplied by the pixel resolution. The side length of the effective calcite cube is calculated from the square root of the projected area.

SI Section 3. Theory

In this section, facilitating the interpretation of experimental results, we adapt and extend theories from previous work[6] of the dissolution kinetics of single, micron-sized, and sparingly soluble particles in solutions so as to establish a generic criterion for distinguishing surface kinetics from thermodynamic control of dissolution. Specifically, we are interested in the auto-dissolution of pristine calcite particles "resting" on an inert, flat supporting subtract. An illustration of the problem is shown in Figure 1 in the main text.

Note that the net flux of materials at the particle interface is necessarily non-zero in the case of particle dissolution. The overall rate of particle dissolution, however, is an interplay between the rate of interfacial reaction *and* how quickly materials are transported to and from the particle surface. In the limiting case where the rate of mass transport is fast and non-rate-limiting then the overall rate of dissolution reflects the surface kinetics. On the other hand, if the rate of mass-transport is slow and rate-determining then the concentration of solutes local to the particle interface is underpinned by the solubility product. The wording "surface kinetic" and "thermodynamic dissolution" is used to distinguish these two limiting cases.

As a particle dissolves in solution the particle size decreases. Conservation of mass means that the concentration of solute at the particle-solution interface is necessarily greater than that in the bulk which results in a diffusional flux of material down the concentration gradient and away from the particle surface. Using an optical microscopy approach, as shown in Figure 1 (A) in the main text, the top-down projection area of the particle can be extracted as a function of time. A general question is, what kinetic information can one extract from the rate of change of the projection area of the particle?

In the following section, we discuss the two limits of dissolution kinetics, namely dissolution limited by either surface kinetics or thermodynamics, and how those may, separately, reflect

the rate of change in particle area as a function of time leading to a key diagnostic for distinguishing the two mechanisms.

"Surface kinetic" or "thermodynamic dissolution"?

To illustrate the two above-described limiting cases of crystal dissolution, "surface kinetic" and "thermodynamic dissolution", we first consider the below-simplified reaction at the particle interface

$$A(s) \underset{k_b}{\overset{k_f}{\rightleftharpoons}} A(aq) \overset{k_{MT}}{\rightarrow} bulk \qquad \textit{Equation S1}$$

where k_f (mol m^{-2} s^{-1}) is the rate constant for the forward (dissolution) reaction, k_b (m s^{-1}) is the backward precipitation rate constant and k_{mt} (m s^{-1}) is the mass transport rate constant. Applying the steady-state approximation[7] to Equation S1 gives

$$[A]_{ss} = \frac{k_f}{k_b + k_{MT}} \qquad \textit{Equation S2}$$

The overall rate of reaction, $flux\ J$, under the steady-state approximation is equal to

$$flux\ J\ (mol\ m^{-2}\ s^{-1}) = [A]_{ss} k_{MT} = \frac{k_f k_{MT}}{k_b + k_{MT}} \qquad \textit{Equation S3}$$

It becomes apparent that, in the case of a *surface kinetic* limitation of rate of dissolution, i.e. $k_{MT} \gg kf\ \&\ k_b$, then Equation S3 becomes

$$flux\ J\ \approx k_f \qquad \textit{Equation S4}$$

However, in the limiting case when diffusion is slow compared to the surface kinetics ($k_{MT} \ll kf\ \&\ k_b$) Equation S3 becomes

$$flux\ J\ \approx \frac{k_f k_{MT}}{k_b} = K_{sp} k_{MT} \qquad \textit{Equation S5}$$

so that the rate is controlled by the solubility product and the rate of diffusion from the surface. This limiting case is termed the "thermodynamic dissolution" in this manuscript. Note that, if a particle dissolves at the thermodynamic limit, the rate-determining mass-transport rate provides a lower-limit for the rate of dissolution and precipitation.

In the following subsection, we adapted from our prior work[6] and we show how the diffusion pattern of calcite particles would differ for the two rate limits: "surface *kinetics*" and "thermodynamic dissolution".

Calcite dissolution

Now, let us consider a calcite particle on a plate placed in an undersaturated solution and the following reaction may be established at the interface

$$CaCO_3(s) \rightleftarrows Ca^{2+}(aq) + CO_3^{2-}(aq) \qquad \textit{Equation S6}$$

Assuming the calcite particle is a cube, which is in approximate agreement with SEM imaging,[6] the number of moles of calcite (n) in the cube is

$$n = \frac{\rho}{M_w} L^3 \qquad \textit{Equation S7}$$

where $\rho = 2.71 \times 10^6$ g m^{-3} is the density of the calcite[8], $M_w = 100.1$ g mol^{-1} is the molecular weight and L is the side length of the calcite cube (m).

Differentiating Equation S7 with respect to time gives an expression in terms of flux of Ca^{2+} and CO_3^{2-} at the particle-solution interface, $j(mol\ s^{-1})$:

$$j(mol\ s^{-1}) = \frac{dn}{dt} = -\frac{3\rho L(t)^2}{M_w}\frac{dL(t)}{dt} \qquad \textit{Equation S8}$$

The minus sign appearing in Equation S8 indicates that the particle size is shrinking as a result of dissolution. Normalising the total flux, j, by the total surface area of the particle gives

$$J = -\frac{\rho}{2R_f M_w}\frac{dL(t)}{dt} \qquad \textit{Equation S9}$$

where J, with units of $mol\ m^{-2}\ s^{-1}$, is the *flux density* of the dissolution reaction and R_f is a surface roughness factor $\left(\text{where } R_f = \frac{\text{actual area}}{\text{geometric area}}\right)$. First, as can be deduced directly from Equation S9, $\boldsymbol{\frac{dL}{dt}}$ **is a constant in the case of a *surface kinetics* limited heterogeneous reaction** since J $(mol\ m^2\ s^{-1})$ is expected to be a constant by definition. Further, by using the chain rule, Equation S9 can be expressed in the form of $\frac{dL(t)^2}{dt}$, where $L(t)^2$ is the projection area of a cube

$$\frac{dL(t)^2}{dt} = 2L(t)\frac{dL(t)}{dt} = -\frac{4R_f M_w J}{\rho}L(t) \qquad \textit{Equation S10}$$

Direct examination of Equation S9 and Equation S10 reveals that, at the *surface limited* rate of dissolution, the rate of change in the projection area of the particle is dependent on the size of the particle which inevitably decreases as dissolution occurs. In contrast, the rate of change in particle length is a constant as a function of time.

Next, in the other limiting case, let us consider the case where the dissolution kinetic occurs at the *thermodynamic limit*. This means that the surface kinetics is *fast* and the concentration of the solution in the layer adjacent to the solid is at thermodynamic equilibrium. Therefore the solute concentration at the particle-solution interface is ***fixed*** by the solubility product. For a cubic particle dissolving on an inert plate, Wong *et al*.[9] report an expression, obtained via 3D finite difference simulation, linking the interfacial solute concentration with the steady-state flux of reaction

$$j_{ss} = 5.45DcL \qquad \textit{Equation S11}$$

where, unsurprisingly, the total flux of material ($mol\ s^{-1}$) across the particle-solution boundary, or in other words, how quickly the particle dissolves is dependent on the size of the particle, L (m^{-1}), the concentration of the solute at the particle-solution interface (c) and the diffusion coefficient of the solute, D ($m^2\ s^{-1}$). This can be expressed in the steady-state flux per unit area, J_{ss}(mol $m^{-2}\ s^{-1}$) by dividing by the geometric area of the cube exposed to the solution.

$$J_{ss} = \frac{1.09Dc}{L} \qquad \textit{Equation S12}$$

Equating Equation S12 with Equation S9 gives an approximate expression for $\frac{dL}{dt}$ at the thermodynamic limit, where R_f in this case is equal to unity since under the thermodynamic limit the rate is dependent on the geometric size of the particle not the surface roughness

$$J_{ss} \approx \frac{1.09Dc}{L(t)} = -\frac{\rho}{2M_w}\frac{dL(t)}{dt} \qquad \textit{Equation S13}$$

Rearranging Equation S13 gives an expression of $\frac{dL(t)}{dt}$ that is proportional to the size of the particle.

$$\frac{dL(t)}{dt} = -\frac{2.18DcM_w}{\rho L(t)} \qquad \textit{Equation S14}$$

Furthermore, analogous to the above, using chain rule Equation S14 can be usefully expressed in the form of $\frac{dL(t)^2}{dt}$, where $L(t)^2$ is the projection area (A) of a cube

$$\frac{dA}{dt} = \frac{dL(t)^2}{dt} = 2L(t)\frac{dL(t)}{dt} = -\frac{4.36DcM_w}{\rho} \qquad \textit{Equation S15}$$

It is clear from the above that, **in the case of particle dissolution occurring at the *thermodynamic limit,* the rate of change of the projection area $\left(\frac{dL(t)^2}{dt}\right)$ of the particle is independent of the size of the particle.** This is in contrast with the above-discussed *surface limited* rate of dissolution where the rate of dissolution of particle length is constant. This distinguishing is generic and will be useful in the Results and Discussion. Note also that if the surface concentration is maintained constant by a mechanism other than being solubility controlled then the value of $\frac{dL(t)^2}{dt}$ will also be constant and the reaction will appear thermodynamic controlled.

SI Section 4. Calcite dissolution into various aqueous solution of NaCl of variable ionic strengths

Using the dissolution pattern, $\frac{dA}{dt}$ versus $\frac{dL}{dt}$, derived for the two limiting cases of particle dissolution outlined in SI Section 3, we next analyse the temporal evolution of calcite single particles under light microscopy.

Figure S1 shows the time dependence of the projection area of individual calcite particles dissolving in various NaCl(aq) solutions. The changes in the projection area and length of particles are shown side-by-side for comparison. As can be seen, dA/dt are linear whereas dL/dt not over the concentrations of NaCl studied, confirming that the dissolution of calcite is

thermodynamically controlled in the absence of magnesium. Pearson's r and R-Squared values from linear line of best fit are shown on each of the plots, further confirming that dA/dt is more linear than dL/dt over all concentrations of NaCl(aq).

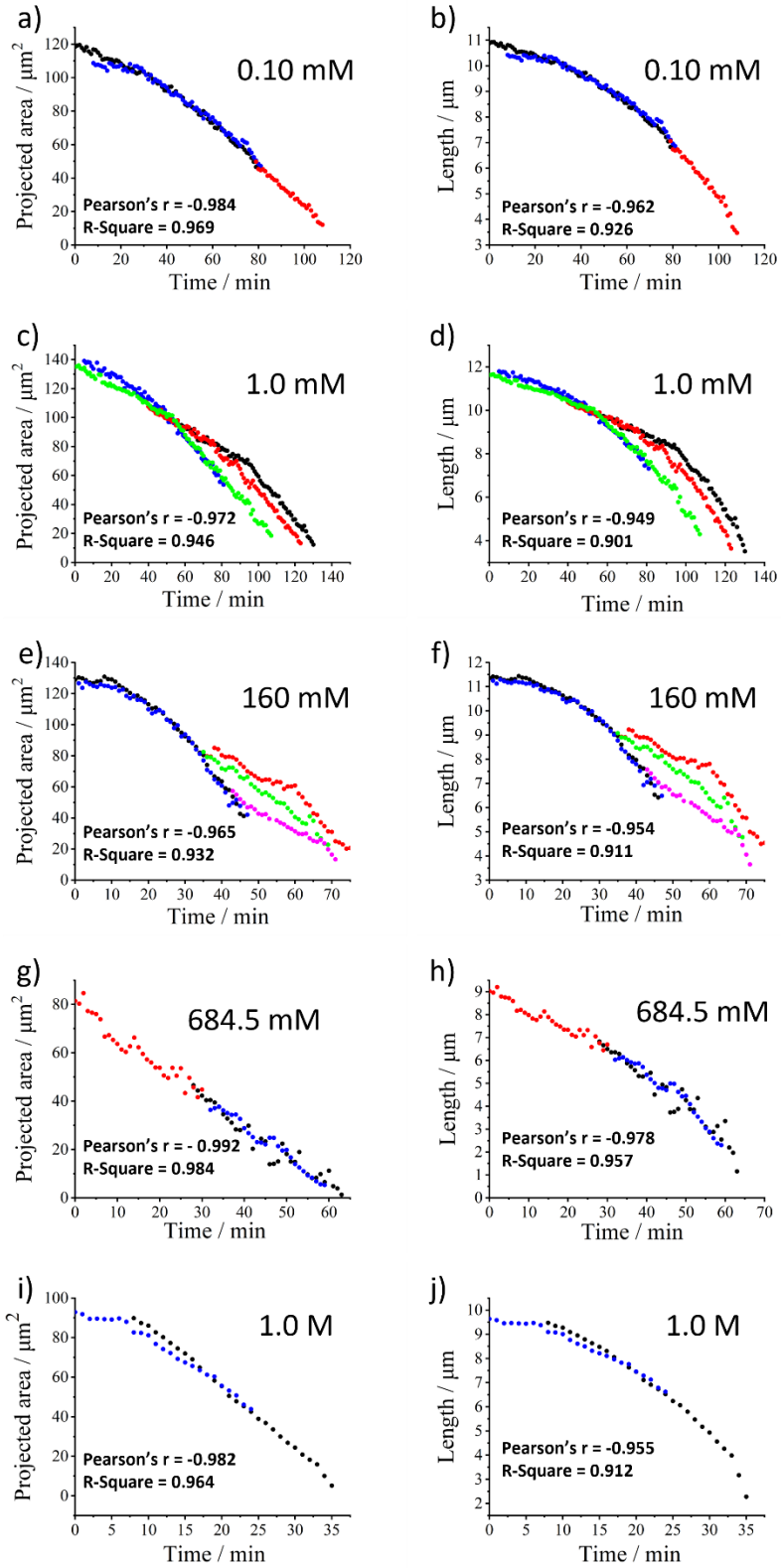

Figure S1. Projected areas and side lengths of calcite particles in NaCl solutions plotted against dissolution time grouped by concentration. The NaCl concentration is labelled on each plot. Also shown on each plot is the Pearson's r and R-Square values obtained from fitting a linear line of best fit through the data. The line of best fit is not shown for clarity of display.

SI Section 5. Solving the calcium carbonate and carbonate equilibria for the dissolution of calcite single-particles

As discussed in the main text, the auto-dissolution of micron-sized single calcite particles occurs at the *thermodynamic* limit as evidenced by the constant value of $\frac{dA}{dt}$ measured from the dissolution experiments. By virtue of considering the steady-state mass-transport flux and the density of the solid particle, the total calcium concentration ($\sum[Ca^{2+}]$) at the particle interface at equilibrium can be calculated from experiment.

Moreover, for a given interfacial concentration of calcite at equilibrium $[Ca^{2+}]_{eq}$ the stoichiometric solubility product K_{sp} for calcite dissolution can be determined by solving the carbonate equilibria, described elsewhere in depth.[6] The list of equations to be solved are:

Chemical equilibria

$$CO_2(aq) + H_2O(l) \overset{K_{a1}}{\rightleftharpoons} H^+(aq) + HCO_3^-(aq) \qquad \textit{Equation S16}$$

$$HCO_3^-(aq) \overset{K_{a2}}{\rightleftharpoons} H^+(aq) + CO_3^{2-}(aq) \qquad \textit{Equation S17}$$

$$H_2O(l) \overset{K_w}{\rightleftharpoons} H^+(aq) + OH^-(aq) \qquad \textit{Equation S18}$$

$$Ca^{2+}(aq) + CO_3^{2-}(aq) \overset{K_{sp}{}^0}{\rightleftharpoons} CaCO_3\ (s) \qquad \textit{Equation S19}$$

$$Ca^{2+}(aq) + CO_3^{2-}(aq) \overset{K_{ip,1}}{\rightleftharpoons} CaCO_3{}^0(aq) \qquad \textit{Equation S 20}$$

$$Ca^{2+}(aq) + HCO_3^-(aq) \overset{K_{ip,2}}{\rightleftharpoons} CaHCO_3{}^+(aq) \qquad \textit{Equation S 21}$$

$$Ca^{2+}(aq) + OH^{-}(aq) \overset{K_{ip,3}}{\rightleftharpoons} CaOH^{+}(aq) \qquad \textit{Equation S 22}$$

Conservation of mass

$$[Ca^{2+}] + [Carb] + [CaCO_3{}^0] + [CaHCO_3{}^+] + [CaOH^+] = [HCO_3^-] + [CO_3^{2-}] + [CO_2(aq)] + [CaHCO_3{}^+] + [CaCO_3{}^0] \qquad \textit{Equation S23}$$

Charge neutrality

$$2[Ca^{2+}] + [CaHCO_3{}^+] + [CaOH^+] + [H^+] = [HCO_3^-] + 2[CO_3^{2-}] + [OH^-] \qquad \textit{Equation S24}$$

The equilibrium constants K_{a1}, K_{a2}, K_{w} are reported extensively as a function of temperature and ionic strength, documented elsewhere[6]. The stoichiometric ion pair association constants $K_{ip,1}$ and $K_{ip,2}$ of calcium (bi)carbonate are, however, more sparely reported. In this work we use the values reported at ionic strength of 0.7 M: $K_{ip,1}$ = 162 M^{-1} and $K_{ip,2}$ = 1.96 M^{-1}.[10] A value of 3.3 M^{-1} at 0.7 M ionic strength $K_{ip,3}$ was calculated using the PHREEQC software where the activity coefficients are estimated using the Davies equation. [Carb] is the total inorganic carbon in the system due to equilibration of the water with the atmosphere. Note that Equation S23 describes conservation of mass and Equation S24 describes the bulk electroneutrality of the solution. The simultaneous equations (Eqn S16-S24) were solved until a specific value $K_{sp}{}^0$, the true stoichiometric solubility product of calcite, results in a total, overall calcium concentration ($\sum[Ca^{2+}]$) that is equal to that inferred at the particle-solution interface in the calcite single-particle dissolution experiment.

SI Section 6. Solving the calcium carbonate and carbonate equilibria in Mucci's 'long-term' experiment

In natural seawater the concentration of magnesium and calcium are present in excess at concentrations of 55 and 10 mM, respectively.[11] To solve the speciation of calcium and carbonate in Mucci's long term equilibration of calcite in seawater[2] (ionic strength = 0.7 M) we need to additionally account for magnesium ion pairs. The list of simultaneous equations to be solve becomes:

Equilibria to be solved

$\begin{pmatrix}\text{Eqn S11}\\ \vdots \\ \text{Eqn S17}\end{pmatrix}$, see above in Section S5

$$Mg^{2+}(aq) + CO_3^{2-}(aq) \overset{K_{ip,4}}{\rightleftharpoons} MgCO_3{}^0(aq) \qquad \textit{Equation S25}$$

$$2Mg^{2+}(aq) + CO_3^{2-}(aq) \overset{K_{ip,5}}{\rightleftharpoons} Mg_2CO_3{}^{2+}(aq) \qquad \textit{Equation S26}$$

$$Mg^{2+}(aq) + Ca^{2+}(aq) + CO_3^{2-}(aq) \overset{K_{ip,6}}{\rightleftharpoons} MgCaCO_3{}^{2+}(aq) \qquad \textit{Equation S27}$$

$$Mg(aq) + OH^{-}(aq) \overset{K_{ip,7}}{\rightleftharpoons} MgOH^{+}(aq) \qquad \textit{Equation S28}$$

Conservation of mass

$$[Ca^{2+}] + [Carb] + [CaCO_3{}^0] + [CaHCO_3{}^+] + [CaOH^+] + [MgCaCO_3{}^{2+}] = [HCO_3^-] + [CO_3^{2-}] + [CO_2(aq)] + [MgCO_3{}^0] + [Mg_2CO_3{}^{2+}] + [MgCaCO_3{}^{2+}] + [CaHCO_3{}^+] + [CaCO_3{}^0] + [Ca\_init]\,; \qquad \textit{Equation S29}$$

$$[Mg^{2+}] + [MgCO_3{}^0] + 2[Mg_2CO_3{}^{2+}] + [MgCaCO_3{}^{2+}] + [MgOH^+] = [Mg\_init] = [SO_4{}^{2-}] = 55mM \qquad \textit{Equation S30}$$

Charge neutrality

$$2[Ca^{2+}] + [CaHCO_3{}^+] + 2[Mg^{2+}] + 2[MgCaCO_3{}^{2+}] + 2[Mg_2CO_3{}^{2+}] + [MgOH^+] + [CaOH^+] + [H^+] = [HCO_3^-] + 2[CO_3^{2-}] + [OH^-] + 2[SO_4{}^{2-}]; \qquad \textit{Equation S31}$$

The stoichiometric ion pair association constants $K_{ip,4}$, $K_{ip,5}$ and $K_{ip,6}$ at 0.7 M ionic strength are 112 M^{-1}, 387 M^{-2} and 1040 M^{-2}, respectively.[10] A value of $K_{ip,7}$ (=89.3 M^{-1}) at 0.7 M ionic strength was calculated using the PHREEQC software. In Mucci's long term equilibrium experiment the experimental apparatus is sealed (closed system) and it is not in equilibrium with the atmosphere. Therefore, [Carb] in the equation above is the total inorganic carbon initially present in the solution. The effects of an *open* and *closed* system with respect to calcite dissolution are discussed elsewhere.[12] $[Ca\_init]$ and $[Mg\_init]$ is the initial concentration of calcium (10 mM) and magnesium (55 mM) present in bulk seawater. Sulphate anions, ${SO_4}^{2-}$, is introduced to preserve charge neutrality of magnesium ions. Note that Equation S29 and Equation S30 describes conservation of mass and Equation S31 describes the bulk electroneutrality of the solution. The simultaneous equations were solved with the true stoichiometric calcite solubility product, ${K_{sp}}^{0}$ (= $[Ca^{2+}][{CO_3}^{2-}]$), as a variable until the apparent stoichiometric calcite solubility product, $K^0_{sp,apparent}$ ($= \sum[Ca^{2+}] \sum[{CO_3}^{2-}]$), equals to 4.4 x 10^{-7} M^2 as reported by Mucci [2].

The true stoichiometric calcite solubility product, ${K_{sp}}^{0}$, that in agreement with Mucci's reported $K^0_{sp,apparent}$ is 5.4 x 10^{-8} M^2. The fraction of calcium and carbonate ions existing as free ions and as ion pairs are summarised in Figure 2 C) in the main manuscript.

Table S1. The chemical speciations in Mucci's seawater solution after 'long term' equilibration with calcite particles.

Chemical speciations	Equilibrium concentrations / M
H^+	1.4 x 10^{-11}
OH^-	4.4 x 10^{-3}
HCO_3^-	7.3 x 10^{-8}
CO_3^{2-}	5.4 x 10^{-6}

Ca^{2+}	9.9×10^{-3}
$CaCO_3^0$	8.7×10^{-6}
$CaHCO_3^+$	1.4×10^{-9}
$CaOH^+$	1.4×10^{-4}
Mg^{2+}	4.0×10^{-2}
$MgCO_3^0$	2.4×10^{-5}
$MgOH^+$	1.5×10^{-2}
$MgCaCO_3^{2+}$	2.2×10^{-6}
$Mg_2CO_3^{2+}$	3.3×10^{-6}
SO_4^{2-}	5.5×10^{-2}

SI Section 7. Calcite dissolution at 0.3 M ionic strength with varying [Mg^{2+}]

Figures S3 and S4 show the time dependence of the projected area of individual calcite particles dissolving in various concentrations of Mg^{2+} at 0.3 M ionic strength. The changes in the projection area and length of particles are shown side-by-side for comparison. As can be seen, over all the concentrations of Mg^{2+} studied, 0 mM to 100 mM, dA/dt is linear thus confirming that the dissolution of calcite in the presence of Mg^{2+} is apparently thermodynamically controlled, as seen in the absence of Mg^{2+}. Note the slight deviations in dA/dt close to the complete dissolution of the particles (ca. < 20 μm^2) is likely due to the shift of the particle away from the optical focal plane.

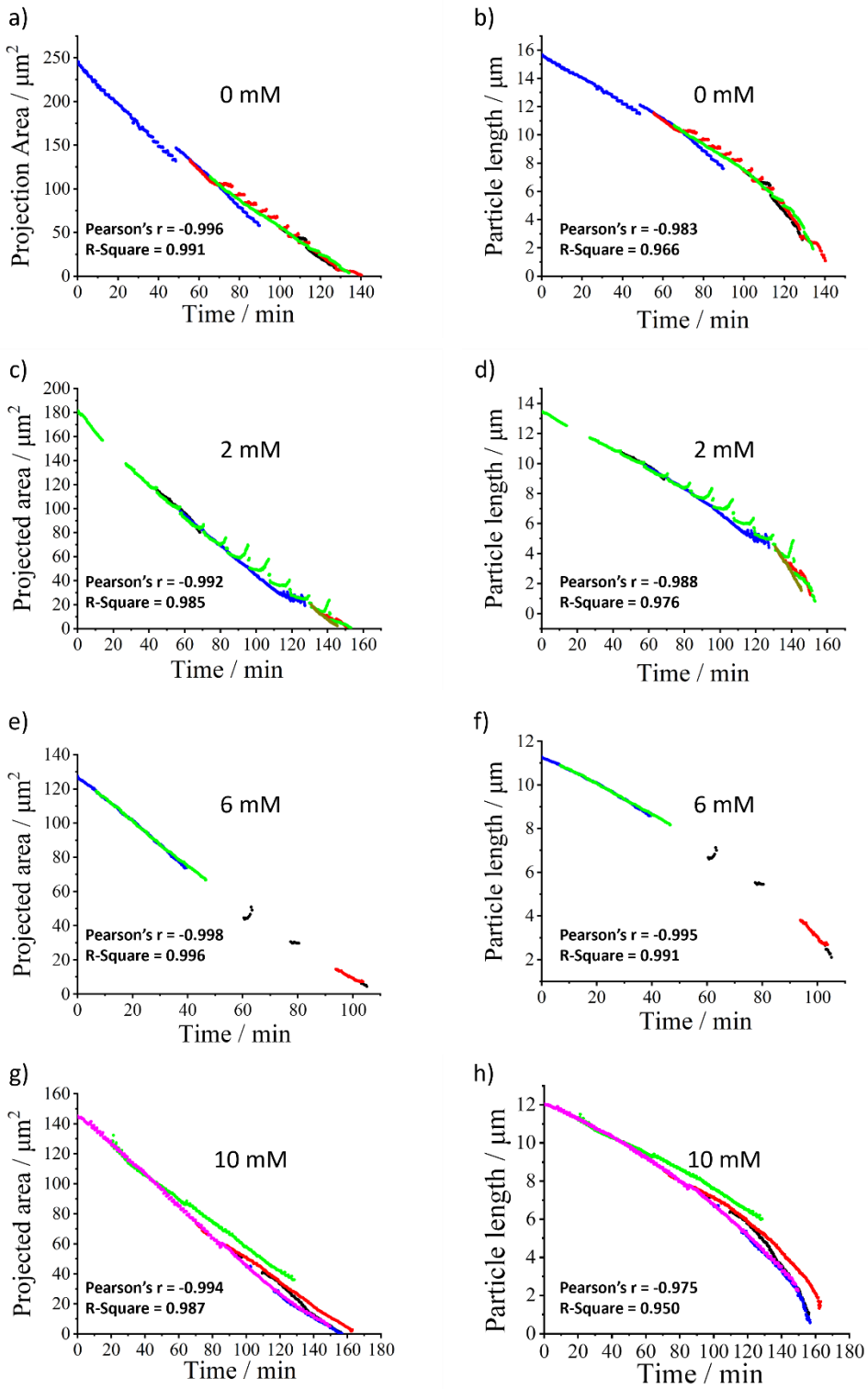

Figure S3. Projected areas and side lengths of dissolving calcite against time for different concentrations (0, 2, 6, 10 mM) of magnesium salt present. The concentration of Mg^{2+} is labelled on each graph. Also shown on each plot is the Pearson's r and R-Square values obtained from fitting a linear line of best fit through the data. The line of best fit is not shown for clarity of display.

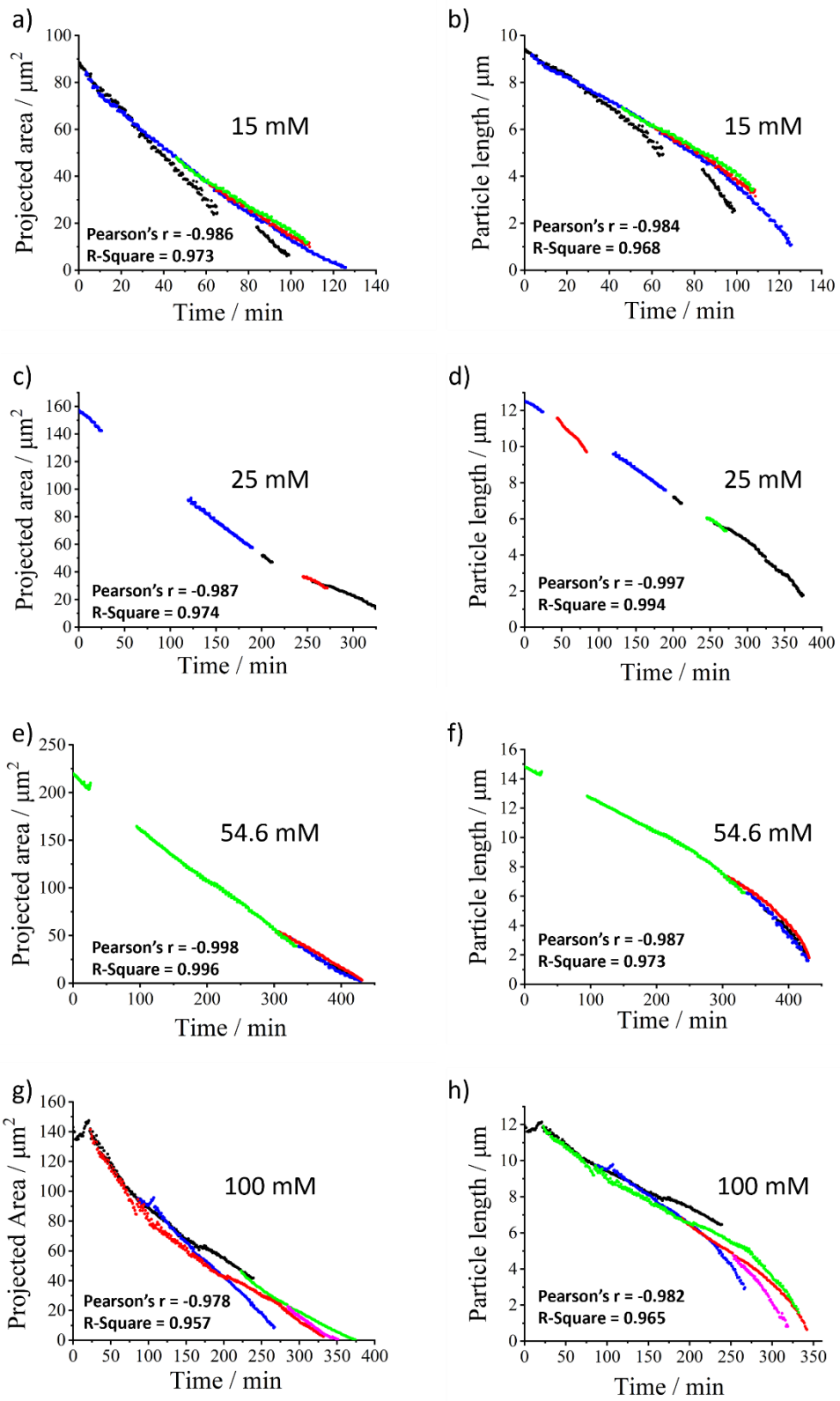

Figure S4. Projected areas and side lengths of dissolving calcite against time for different concentrations (15, 25, 54.6, 100 mM) of magnesium salt present. The concentration of Mg^{2+} is labelled on each graph. Also shown on each plot is the Pearson's r and R-Square values obtained from fitting a linear line of best fit through the data. The line of best fit is not shown for clarity of display.

SI Section 8: Kinetic magnesium inhibition mechanism

In this section, we explore an alternative calcite dissolution inhibition mechanism to that presented in the main text, where the presence of Mg^{2+} ***lowers*** the rate-constants of calcite dissolution/precipitation, an alternative mechanism to that of adsorption on the calcite surface as discussed in the main text.

$$CaCO_3(s) \rightleftharpoons Ca^{2+} + CO_3^{2-} \qquad \textit{Equation S32}$$

The 1D model and boundary conditions in consideration are illustrated in Figure S5 a). The simulation was discretised using the finite difference method and solved backwards-implicitly using a LU decomposition method described elsewhere[13]. The interfacial flux (j) at the particle interface is defined by

$$flux\ j\ (mol\ m^{-2}\ s^{-}) = -D_A \frac{d[A]}{dx}\Big|_{x=0} = k_f - k_b[A]_{x=0} \quad \textit{Equation S33}$$

where D_A is the diffusion coefficient of species A ($1x10^{-9}$ m^2 s^{-1}). Figure S2 b) shows the instantaneous flux at the particle interface as a function of k_f at time t = 10 s. Note that K_{sp} is constant and $k_b = k_f / K_{sp}$ so that k_b increases proportionally with k_f. The mass-transport rate constant k_{MT} for a 1-D system is equal to the Cottrell equation $\left(= \sqrt{\frac{D}{\pi t}}\right)$. In the limit of a high k_f (i.e. k_f & k_b >> K_{MT}), Equation S3 reduces to $K_{sp}k_{MT}$ (Equation S5) and the analytical expression of flux j ($=K_{sp}\sqrt{\frac{D}{\pi t}}$) is in excellent agreement with the simulation result shown in Figure S5 b).

As can be seen in Figures S5 b), a six-fold slower in the overall observed rate of dissolution (mol m^{-2} s^{-1}) as seen in Figure 6 would result in a transition from the thermodynamic regime into either the mixed-regime or the surface limited regime. This was not seen since dA/dt remains linear over all concentrations of Mg^{2+}. We therefore conclude that the alternative Mg^{2+} inhibition mechanism discussion herein is unlikely the case.

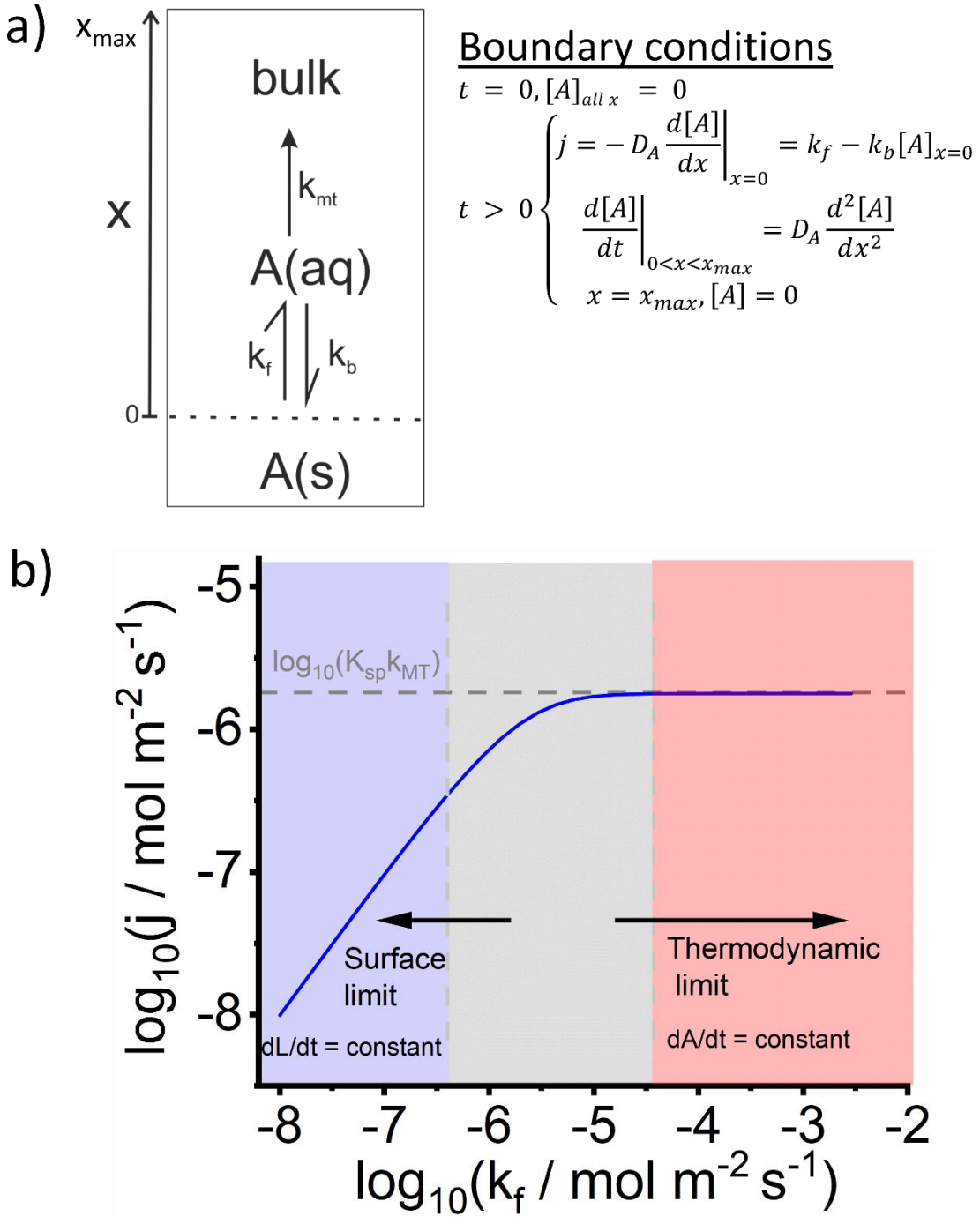

Figure S5. Schematic of the predicted flux (see SI Section 6) vs k_f (mol m^{-2} s^{-1}). a) schematic of the model and boundary conditions. b) flux at the particle interface as a function of the forward dissolution rate constant k_f. Other simulation parameters: K_{sp} = 1 mol m^{-3}, $k_b = k_f/K_{sp}$, D_A = 1x10^{-10} m^2 s^{-1}.

SI section 9: partially blocked surface

In the main manuscript the partial coverage of magnesium on calcite surfaces is suggested to behave analogously to a 'partially blocked electrode' surface[14-16]. In the case of the latter, illustrated in Figure S6 (a), the surface concentration of the analyte on an electrode surface is consumed at an unperturbed (active) electrode surface. The 'blocked' sites are inert and do not perturb the concentration of analyte. The perturbation of the analyte concentration at the active surface causes materials to diffuse from the semi-infinite bulk, shown by the dotted contour lines. As the material near the electrode surface is fully consumed diffusion occurs from further away from the electrode which causes an increase in the diffusion layer thickness (δ) with time. The diffusion layer overlaps when the diffusion layer thickness δ becomes larger than d (the separation between different sites) in the long-time limit or if the separation of the sites becomes smaller (d << δ).[14-16] This scenario is illustrated in Figure S6 a) where the consumption of the analyte is uniform across all surfaces (active and blocked).

In the case of the calcite dissolution in the presence of Mg^{2+}, on a molecular scale, the surface calcite crystalline units are either pristine or with magnesium physisorbed. The adsorption of magnesium appears to lower the effective solubility product of calcite by *ca* a factor of 6 as shown in Figure 3 C). However, since the rate of dissolution of calcite in the presence of magnesium under the concentrations studied remains at the thermodynamic limit then the interfacial concentration of calcium at different surface sites, with and without magnesium adsorption, is necessary *different* as illustrated in Figure S6 b) by the colours of the concentration contour lines. Since in the case of Langmuirian adsorption, the probability of adsorption is similar at all sites then the separation (d) between the pristine and Mg^{2+}(ads) surface sites is on the order of Å. Note that this is much smaller than the hundreds of microns of diffusion layer thickness ($\delta \approx \sqrt{Dt}$) over the timescale of calcite dissolution (~hours). Therefore, to a good approximation, at distances far away from the calcite interface the

diffusion layer between two different calcite surface sites overlaps very significantly and thus the ***overall*** concentration of calcium at equilibrium *at the surface* is intuitively perceived as the weighted sum of the individual sites as shown in Equation 19 in the main text.

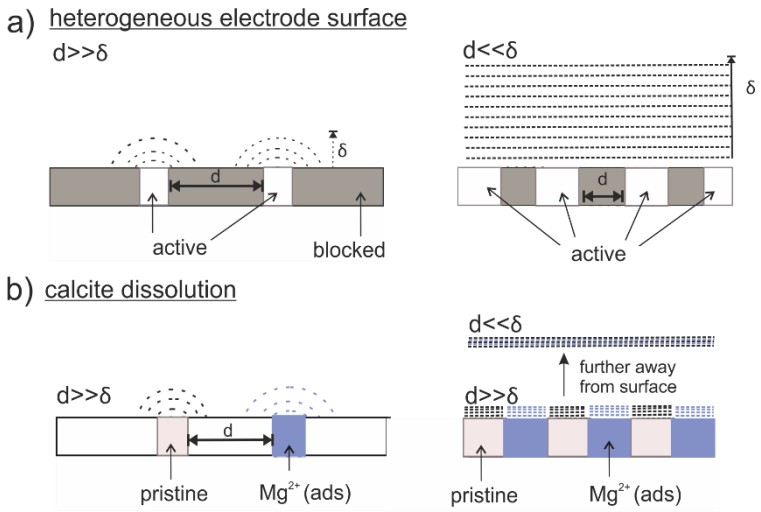

Figure S6. ***a)*** *Illustration of the diffusion layer at the onset of electrolysis in the case of a partially blocked electrode.* ***b)*** *analogue representation of the surface calcite site in the presence of Mg^{2+}(aq). The dotted lines represent the concentration contour lines.*

1. J. W. Morse, A. Mucci and F. J. Millero, *Geochimica et Cosmochimica Acta*, 1980, 44, 85-94.
2. A. Mucci, *American Journal of Science*, 1983, 283, 780-799.
3. K. Azetsu-Scott, A. Clarke, K. Falkner, J. Hamilton, E. P. Jones, C. Lee, B. Petrie, S. Prinsenberg, M. Starr and P. Yeats, *Journal of Geophysical Research: Oceans*, 2010, 115.
4. R. A. Feely, C. L. Sabine, K. Lee, W. Berelson, J. Kleypas, V. J. Fabry and F. J. Millero, *Science*, 2004, 305, 362-366.
5. S. N. Chung, K. Lee, R. Feely, C. Sabine, F. Millero, R. Wanninkhof, J. Bullister, R. Key and T. H. Peng, *Global Biogeochemical Cycles*, 2003, 17.
6. X. Fan, C. Batchelor-McAuley, M. Yang and R. G. Compton, *ACS Measurement Science Au*, 2022, 2, 422-429.
7. P. W. Atkins, J. De Paula and J. Keeler, *Atkins' physical chemistry*, Oxford university press, 2023.
8. W. M. Haynes, *CRC Handbook of Chemistry and Physics*, CRC press, 2016.
9. R. Wong, C. Batchelor-McAuley, M. Yang and R. G. Compton, *Journal of Electroanalytical Chemistry*, 2021, 903, 115818.
10. R. Pytkowicz and J. Hawley, *Limnology and Oceanography*, 1974, 19, 223-234.
11. F. J. Millero, R. Feistel, D. G. Wright and T. J. McDougall, *Deep Sea Research Part I: Oceanographic Research Papers*, 2008, 55, 50-72.
12. C. Batchelor-McAuley, M. Yang, R. E. Rickaby and R. G. Compton, *Chemistry–A European Journal*, 2022, 28, e202202290.
13. R. G. Compton, E. Kätelhön, K. R. Ward and E. Laborda, *Understanding Voltammetry: Simulation of Electrode Processes*, World Scientific, 2020.
14. B. A. Brookes, T. J. Davies, A. C. Fisher, R. G. Evans, S. J. Wilkins, K. Yunus, J. D. Wadhawan and R. G. Compton, *The Journal of Physical Chemistry B*, 2003, 107, 1616-1627.
15. T. J. Davies, C. E. Banks and R. G. Compton, *Journal of Solid State Electrochemistry*, 2005, 9, 797-808.
16. T. J. Davies, R. R. Moore, C. E. Banks and R. G. Compton, *Journal of Electroanalytical Chemistry*, 2004, 574, 123-152.